Wind energy support structures

Renewable Energies Offshore – Guedes Soares (Ed.)
© 2015 Taylor & Francis Group, London, ISBN: 978-1-138-02871-5

A study of fatigue crack growth in offshore wind monopile parent steel in air and seawater

O. Adedipe & F. Brennan
Cranfield University, Bedfordshire, UK

ABSTRACT: Offshore wind turbines supported on monopile structures have significantly different structural dynamic response characteristics compared to oil and gas structures due to the structural stiffness and machine loading characteristics. Therefore, the effect of corrosion assisted fatigue damage in offshore wind turbine support structures needs to be researched and better understood for reliable operation of the structures in service. This paper presents constant amplitude fatigue crack propagation tests conducted on representative Compact Tension specimens (CT) in air and in laboratory simulated free corrosion seawater environment similar to what might be experienced by steel monopile wind turbine support structures. Crack growth rates were shown to be faster in seawater than in air across all the applied cyclic stress intensity factor ranges tested. Mean stress effect on fatigue crack growth was accounted for at stress ratios of −1 to 0.6 using various mean stress models. Significant difference in the predicted results is discussed.

1 INTRODUCTION

Offshore wind turbine monopile structures are fabricated from rolled steel plates welded both longitudinally and by circumferential or splice welding processes. In spite of the level of quality control measures applied during fabrication and welding, there is still the potential for defects at the intersection between the parent material and the weld region which could result in some significant local stress concentrations. Due to the synergistic effects of a corrosive environment, machine, wind and wave loading encountered by the structures in service, fatigue cracks can initiate from the weld region and propagate progressively to failure. Fatigue cracks in offshore wind farm monopiles therefore need to be discovered and sized by reliable inspection and monitoring techniques to ensure economical and safe operation of the structures.

Considering the significant difference in the loading regime, environmental conditions and low profit margins associated with offshore wind industries compared with the oil and gas sector, there is need to update the corrosion fatigue database to optimise cost and fatigue strength associated with the structures (Brennan 2014). Due to the time dependent mechanisms which occur during the corrosion fatigue process, corrosion fatigue experiments in monopile structure representative materials therefore need to be conducted at the dominant response frequency of offshore wind monopile structures. Studies have revealed that the dominant frequency of the support structure is in the range of 0.3–0.4 Hz but closer to 0.3 Hz which corresponds to the first bending mode frequency of the wind turbine structure. Details can be found in References (Bhattacharya et al. 2013, Lombardi et al. 2013, Andersen et al. 2012). Based on these studies, the dominant frequency of 0.3 Hz was chosen for testing in this study. In corrosion fatigue situations, lower load frequencies are more detrimental due to longer time a crack tip is exposed to electrochemical corrosion elements per cycle.

Several research studies on corrosion fatigue behaviour in offshore oil and gas structures have been conducted on representative material such as BS4360 50D steel at cyclic load frequency range of 0.1–0.2 Hz and under cathodic protections (Scott et al. 1983, Thorpe et al. 1983, Wildschurt et al. 1978, Haagensen et al. 1978, Booth 1978, Berge 1978, Solli 1978, Bardall et al. 1978, Haagensen & Dagestad 1978). A significant number of these experimental programmes were conducted three decades ago, but since then relatively little has been published. These findings have generally revealed that crack growth rates are faster in seawater than in air irrespective of the level of cathodic protection.

As mentioned earlier, offshore wind turbines have significantly different structural dynamic response characteristic compared to oil and gas structures. Therefore, knowledge of the loading frequency experienced by these structures is very important in order to form a basis for laboratory test programmes. Structural dynamic response of offshore wind turbines have been reported to depend on the soil structure interaction stiffness (soft-soft, soft-stiff and stiff-stiff), turbine size, water depth, monopile diameter and stiffness (Bhattacharya et al. 2013, Lombardi et al. 2013,

Andersen et al. 2012). In these studies, the first order dynamic frequency of monopile support structures was found to lie between the rotor frequency and blade passing frequency generally within the range of 0.3–0.4 Hz.

Free corrosion conditions inside and outside the monopile structures might occur due to the loss in corrosion protection over time coupled with mitigating the risks associated with cathodic protection such as production of hydrogen, chlorine and change in water chemistry. Therefore it is essential to carry out research on free corrosion fatigue conditions to advance more effective and realistic long-term service life predictions. To this end, tests were conducted in the study in air and at 0.3 Hz in laboratory simulated seawater under free corrosion condition using Compact Tension test specimens. It is worth mentioning that the global effect of corrosion with respect to reduction in thickness of the test specimens was not considered. Only the corrosion fatigue crack propagation results are reported. The mechanism of corrosion effect under high stress and low stress conditions were studied for in-air and simulated seawater using various mean stress models. The selection of appropriate models and derived material response data are compulsory when a reliable fatigue life prediction modelling is required. Some of the mean stress models are discussed in a later section.

In welded structures, the presence of weld induced residual stresses will result in higher mean stress or higher R ratio such that the applied stress cycle at the vicinity of the crack at a lower R ratio is actually under a higher R ratio. Therefore, for a conservative approach in predicting the lifetime of the structure, the crack growth data obtained at a higher R ratio can be considered as the relevant data for fatigue life estimation. However, the effect of welding was not considered in this study as tests were conducted on parent materials.

2 FATIGUE CRACK PROPAGATION MODELS

The most widely used fatigue crack propagation model was introduced based on the concept of linear elastic fracture mechanics by Paris & Erdogan (1963) as a relationship between crack growth rate (*da/dN*) and cyclic stress intensity factor range *(*ΔK), such that

$$\frac{da}{dN} = C(\Delta K)^m \tag{1}$$

Where *C* and *m* are material constants.

The Paris relationship is limited to only region II of fatigue crack growth but at threshold (region I) and during unstable crack growth (region III), the Paris Law is not effective. Another limitation of the Paris model is its inability to predict the effect of stress ratio on fatigue crack growth. However, many models have been proposed to consider R ratio effects. The intention of these models is to reduce the number of experimental data required to obtain material constants for different R-ratios. Some of the commonly used models are briefly discussed in this paper.

Mean stress effects are generally expressed in terms of the ratio of the minimum to the maximum applied stress a material is subjected to during cyclic loading. For most steels subjected to different stress ratios, a number of parallel straight lines are produced on a *da/dN* versus ΔK plot and result in the same *m* values but specific *C* values (Beden et al. 2009). The well-known crack closure concept was proposed by Elber (1971) by using the effective stress intensity factor range as the crack driving parameter responsible for mean stress effect. The model was formulated as

$$\Delta K_{eff} = U\Delta K \tag{2}$$

Where *U* is the crack closure ratio which is expressed as

$$U = \frac{K_{\max} - K_{op}}{K_{\max} - K_{\min}} \tag{3}$$

Where K_{op} is the opening stress intensity factor at a crack opening stress σ_{op}. K_{op} is usually derived at the crack opening load corresponding to 2% deviation from the load versus displacement relationship as recommended in the ASTM E647 (ASTM E647 2008). However, it is difficult to determine K_{op} due to its relationship to R ratio (Zhan et al. 2014).

An empirical model which incorporates mean stress effect was also developed by Walker (1970). Walker's model can be directly fitted to crack growth data at different mean stresses. The model is expressed as

$$\frac{da}{dN} = C\left(\frac{\Delta K}{(1-R)^{(1-y)}}\right)^m \tag{4}$$

where *y* is the Walker's exponent. The values of y for metals range from 0.3 to approximately 1 with an average value of 0.5. Lower values of *y* indicate a stronger influence of R on fatigue crack growth and vice versa.

Forman (1972) introduced a modified Paris and Walker's equations which is capable of representing data for both region II and region III of fatigue crack growth. Forman's equation can be written as

$$\frac{da}{dN} = \frac{C(\Delta K)^m}{(1-R)K_c - \Delta K} = \frac{C(\Delta K)^m}{(1-R)(K_c - K_{\max})} \tag{5}$$

where K_c is the critical stress intensity factor or the fracture toughness of the material under consideration. As $K_{\max}$ approaches K_c the denominator of equation (5) approaches zero and the crack growth tends to infinity.

Some authors have pointed out some inadequacies in the crack closure model proposed by Elber. McClung (1991), reported that the theory of crack closure should be attributed to the three regions of fatigue crack growth. Dinda & Kujawski (2004), also

mentioned that crack closure concept is not the only method that can be used to predict fatigue crack growth accurately. A correlation which depicts the effect of R ratio by using the crack driving force termed K^* without a need for collection of crack closure data was developed by Kujawski (2001) and is expressed as

$$\Delta K^* = \left(K_{\max} \Delta K^+\right)^{0.5} \tag{6}$$

Equation 6 was later modified as

$$\Delta K^* = \left(K_{\max}\right)^{\alpha} \left(\Delta K^+\right)^{1-\alpha} \tag{7}$$

Where ΔK^+ is the positive part of the range of applied stress intensity factor (SIF), K_{max} is the corresponding maximum value of the applied SIF and α is a parameter which is determined from the average of slopes of the logarithmic plots of K_{max} versus K^+ for a given constant crack growth rate.

Huang & Moan (2007) also proposed a correlation which is capable of predicting fatigue crack growth at different stress ratios using the material response data derived at R ratio of 0. The correlations is expressed as

$$\frac{da}{dN} = C_0 \left(M\Delta K\right)^{m0} \tag{8}$$

Where C_0 and m_0 are the determined material constants at R-Ratio of 0,

$$M = \begin{cases} \left(1-R\right)^{-\beta_1}, & -5 \le R < 0 \\ \left(1-R\right)^{-\beta}, & 0 \le R < 0.5 \\ \left(1.05 - 1.4R + 0.6R^2\right)^{-\beta}, & 0.5 \le R < 1 \end{cases} \tag{9}$$

Where $\beta_1 = 1.2\beta$, and β, β_1, are material constants. The constant β was assigned a value 0.7 for aluminium and steels when there is insufficient experimental data (Huang & Moan 2007, Weng et al. 2013). Details of this can be found in (Huang & Moan 2007).

Recently, Zhan et al. (2014) proposed a correlation similar to that developed by Huang and Moan, to account for mean stress effect on crack growth rate at stress ratios in the range of $-1 \le R \le 1$ by applying the experimentally obtained material response data at R-ratio of 0. The model can be expressed as

$$\frac{da}{dN} = C_0 \left(\phi\Delta K\right)^{m0} \tag{10}$$

where Ø is a correction factor which depends on the R ratio and is expressed as

$$\phi = \exp(\alpha R) \tag{11}$$

α was set at 0.65 for low strength metallic materials, 0.75 for high strength metallic materials such as Ti-alloys and 0.65 for all other metallic materials.

Some of the models discussed above have been applied in this study to account for mean stress effect on fatigue crack growth in air and in laboratory simulated seawater. Details of this will be given later.

Table 1. Material composition of S355J2+N steel.

Element	Composition %	Specification %
C	0.16	0.20 max
Si	0.38	0.55 max
Mn	1.42	1.60 max
P	0.013	0.025 max
S	0.006	0.025 max
Cr	0.3	
Mo	0.08	
Ni	0.3	
Al	0.015	
Cu	0.4	
Nb	0.003	
B	0.0008	
Ti	0.05	
V	0.1	

Table 2. Mechanical Properties of S355J2+N steel.

Yield strength	Tensile strength	Elongation	Charpy value
MPa	MPa	%	at −20°C
345 min	470–630	20	176

3 MATERIAL

The material used for this study was a 20 mm thick plate of EN10025-2:2004 S355J2 + N steel. 16 mm thick Compact Tension specimens were extracted from the plate and were designed according to the specification set out in ASTM E647 (ASTM E647 2008). The notch was machined by spark erosion perpendicular to the rolling direction of the plate. The material composition and the mechanical properties are set out in Tables 1 and 2.

4 EXPERIMENTAL METHOD

Fatigue tests were conducted in accordance with the ASTM E647 on two 100 kN capacity servo – hydraulic fatigue machines. The specimens were precracked in air with the load gradually reduced as recommended in ASTM E647. Constant amplitude sinusoidal loads were applied on the specimens at a load frequency of 2–5 Hz in air at ambient temperature of about 21°C and at a load frequency of 0.3 Hz in the simulated seawater. The seawater temperature was maintained at 8–10°C. The tests were conducted at the load ratio of 0.1 in both environments. Prior to testing in a corrosive environment, the specimen was pre-exposed for 48 hours under no load to increase crack growth rate.

The simulated seawater was continuously circulated past the fully immersed specimen through a designed Perspex environmental chamber at the rate of 3 litres/minute. The seawater pH was regularly checked through a digital pH meter and was maintained at the range of 7.78 to 8.1.

Crack lengths were monitored by direct current potential difference (DCPD), digital camera and back face strain (BFS) methods (Adedipe et al. in prep.). A strain gauge was installed on the back of each specimen to measure the strain values as the fatigue cracks propagate and was protected in the seawater environment by coating the surface with Neoprene rubber coating material. The two types of waveforms used in this study are the single wave matrix type which is the commonly used uninterrupted sinusoidal waveform and the loop type waveform which was programmed to hold for few seconds at the test mean load to allow a stable reading from the strain gauge.

5 RESULTS AND DISCUSSION

The results are presented as plots of crack lengths versus number of cycles and crack growth rates versus cyclic stress intensity factor range as depicted in Figures 1 to 4. Crack growth rates were determined from the plots of crack lengths versus number of cycles using the seven point incremental polynomial method (ASTM E647 2008). Figure 1 shows the crack growth results observed in air at two different types of waveforms and loading frequencies. The crack growth results obtained in seawater are plotted in Figure 2.

Crack propagation results in air were recorded over 366,000 cycles for the single wave matrix method, while the specimen tested at loop control waveform method consumed approximately 372,000 cycles regardless of the difference in loading frequency. It can also be seen as shown in Figure 1 and Figure 3 that the curves are similar over the range of loading cycles. This implies that air test can be conducted at higher load frequency to reduce experimental time. An explanation for the fair difference in number of expended cycles could be as a result of the accumulated waveform interruption in the loop control method as previously mentioned.

Figure 4 compares the air and free corrosion condition results. At lower ΔK, the crack growth result in air was somewhat similar to that in seawater. This might be as a result of the lesser effects of corrosion elements entering the crack tip during the early stage of crack propagation. Another explanation for this is the time dependent mechanisms associated with corrosion process which may not be fully effective at lower stress ratio due to crack closure effects coupled with the effect of the remaining uncracked ligament of the specimen. The observed scatter in the seawater data compared with air data especially at lower ΔK as shown in Figure 4 was due to the number of recorded data points in the seawater test.

At mid-way of the crack propagation, crack growth rate in seawater increased by approximately a factor of 3 relative to air. The effect of the pre-exposed period could be the underlying reason for such and at a stage in the crack growth process, it is expected that a significant amount of the corrosive elements will dominate the bulk of the region around crack tip causing higher

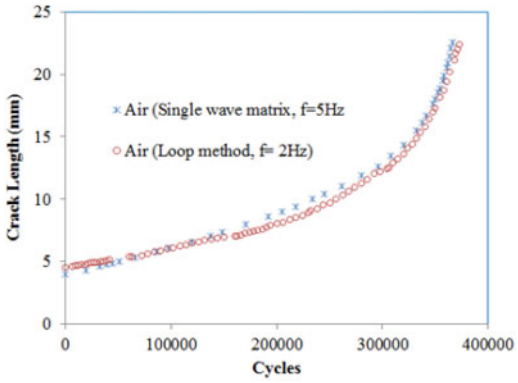

Figure 1. Fatigue crack growth of CT specimens in air.

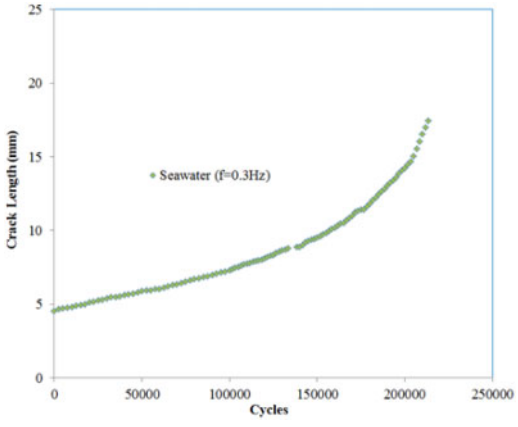

Figure 2. Fatigue crack growth of CT specimen in seawater.

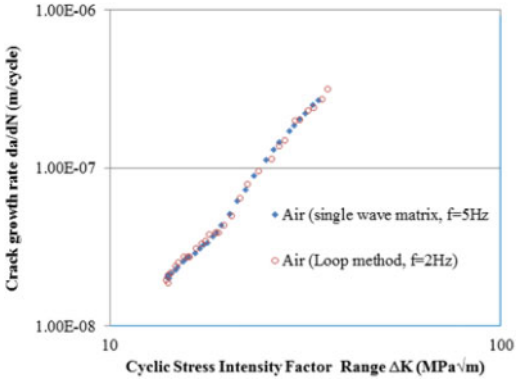

Figure 3. Crack growth rate of CT specimens in air.

crack growth. Results generally revealed that crack growth rates in seawater increased by a factor of 2 and 4 relative to air at lower and higher range of applied stress intensity factors respectively. The magnitude of the increase in crack growth rate at higher ΔK may

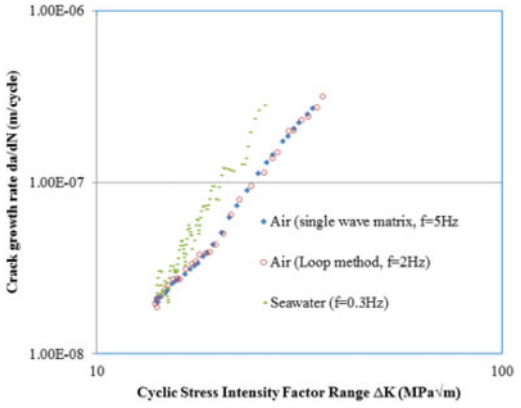

Figure 4. Comparison of crack growth rate in air and seawater.

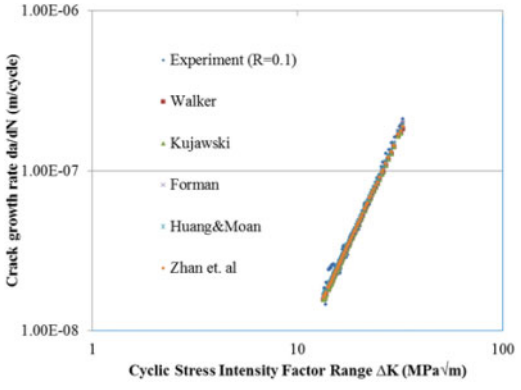

Figure 5. Comparison of predicted crack growth rate at R ratio of 0.1 in air.

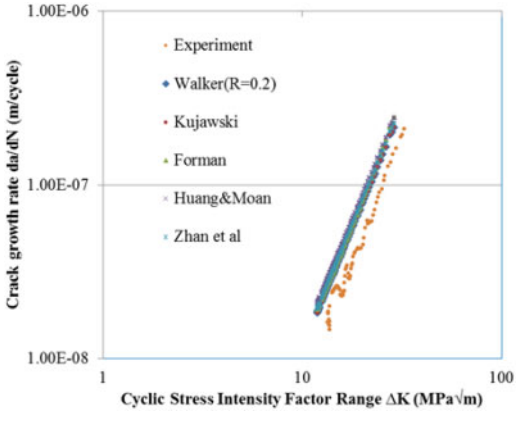

Figure 6. Comparison of predicted crack growth rate at R ratio of 0.2 in air.

be directly attributed to the degree of metal removal at the highly stressed region around the crack tip. This phenomenon implies that cycling at lower frequency in seawater is damaging due to higher proportion of time

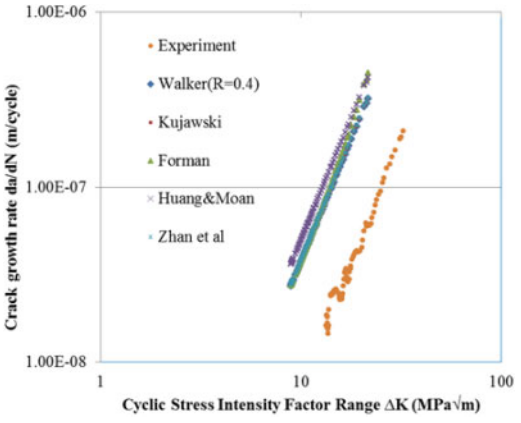

Figure 7. Comparison of predicted crack growth rate at R ratio of 0.4 in air.

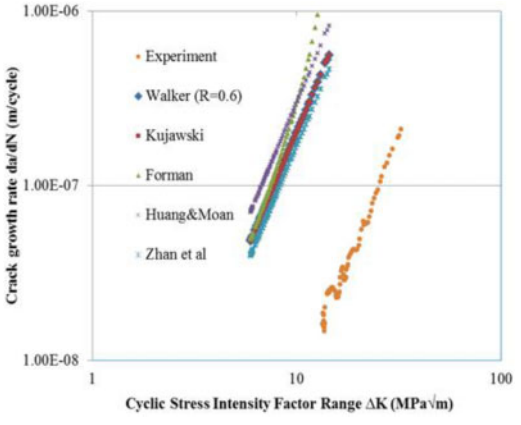

Figure 8. Comparison of predicted crack growth rate at R ratio of 0.6 in air.

in which the crack tip is exposed to the harsh environment causing a significant amount of electrochemical reaction of steel and seawater.

Figures 5 to 19 describe the effects of R ratio on fatigue crack growth using different mean stress models. Experimental crack growth result obtained at R ratio of 0.1 was used as a baseline in the modelling exercise. Mean stress effect was modelled in air and seawater using Walker's, Forman's, Kujawski's, Zhan et al. and Huang and Moans models (Equations 4 to 11). The predicted crack growth rates in air for different R ratios are shown in Figure 5 to Figure 10. Included in the Figures are the experimental results obtained at R ratio of 0.1. It can be seen that the curves move to the left of the baseline ($R = 0.1$) for R increasing cases while for $R \leq 0$, the predicted curves shifts to the right of the baseline. Crack growth rates were higher at higher stress ratios with lower stress intensity factor thresholds and vice versa. This concept is

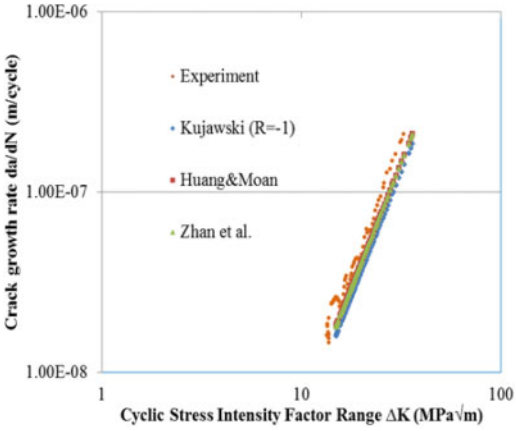

Figure 9. Comparison of predicted crack growth rate at R ratio of −1 in air.

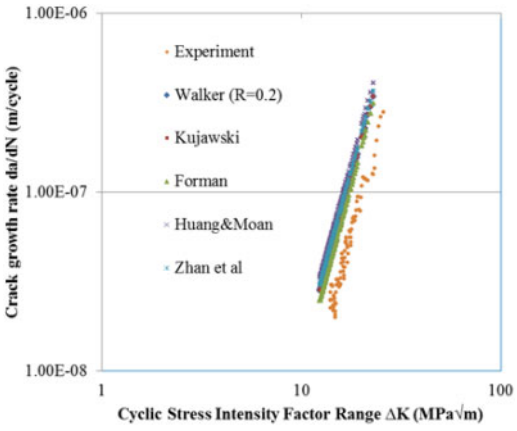

Figure 12. Comparison of predicted crack growth rate at R ratio of 0.2 in seawater.

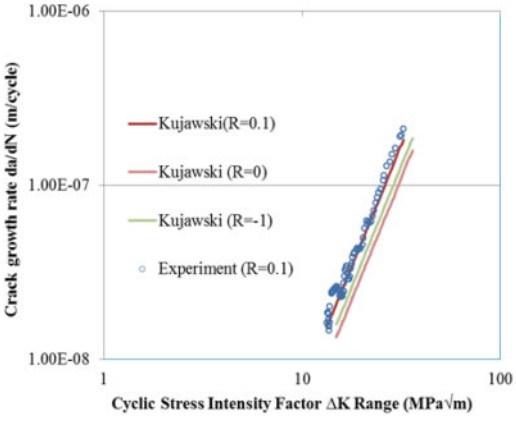

Figure 10. Comparison of predicted crack growth rate in air at R ratios of 0.1, 0 and −1.

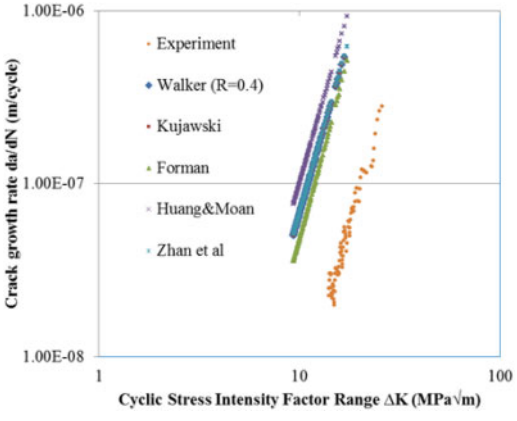

Figure 13. Comparison of predicted crack growth rate at R ratio of 0.4 in seawater.

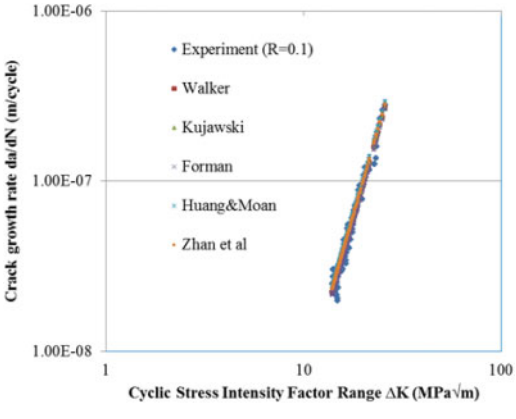

Figure 11. Comparison of predicted crack growth rate at R ratio of 0.1 in seawater.

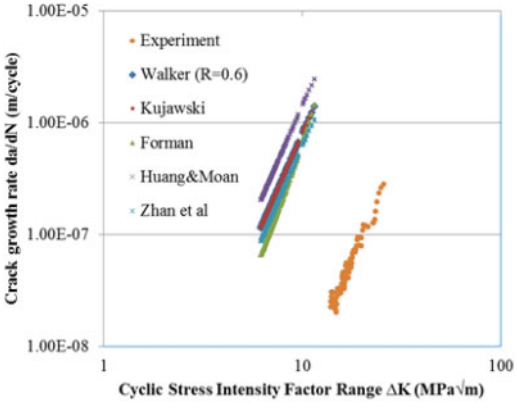

Figure 14. Comparison of predicted crack growth rate at R ratio of 0.6 in seawater.

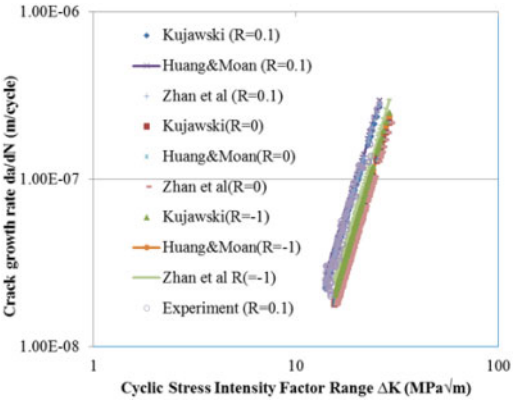

Figure 15. Comparison of predicted crack growth rate in seawater at R ratios of 0.1, 0 and −1.

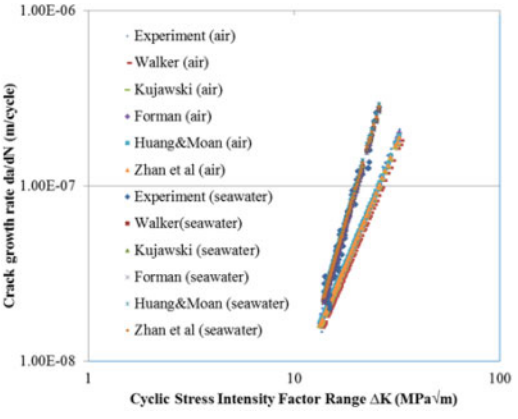

Figure 16. Comparison of predicted crack growth rate in air and seawater at R ratio of 0.1.

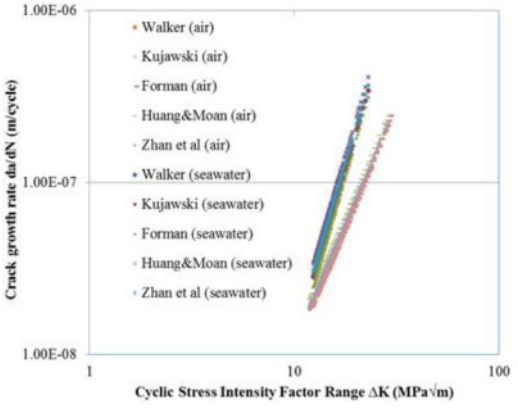

Figure 17. Comparison of predicted crack growth rate in air and seawater at R ratio of 0.2.

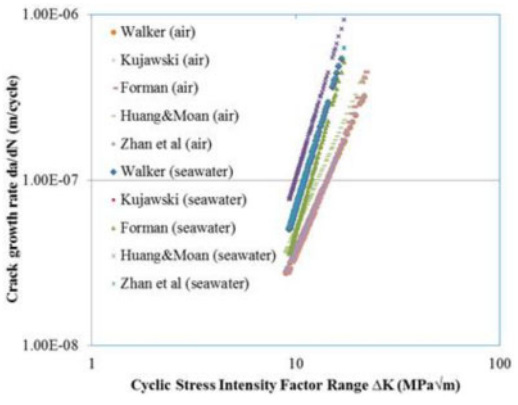

Figure 18. Comparison of predicted crack growth rate in air and seawater at R ratio of 0.4.

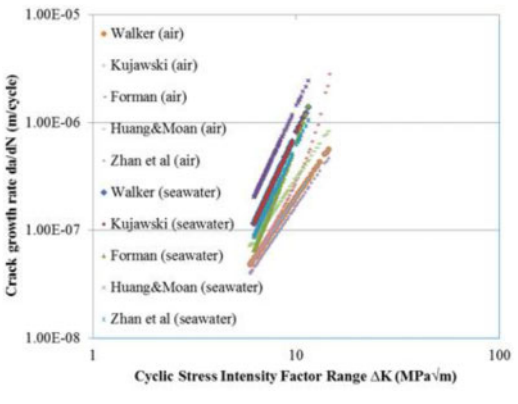

Figure 19. Comparison of predicted crack growth rate in air and seawater at R ratio of 0.6.

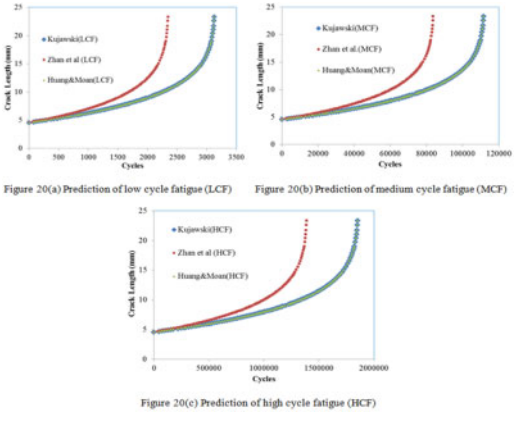

Figure 20. Prediction of low, medium and high cycles fatigue at R-ratio of −1.

a useful engineering procedure due to the time constraints and difficulty in getting experimental data at different R-Ratios. There is a good agreement between Walker's and Kujawski's models for all the R ratios as measured by the same Paris constants regardless of the Walkers exponent. Zhan et al. prediction also agree with Walker's and Kujaswki's up to R ratio of 0.4 but Forman's, Huang and Moan models only agree with the other predicted curves up to R ratio of 0.2. These results are shown in Figures 5, 6 and 7.

At R ratio of 0.6 (Figure 8), Forman's and Huang and Moan predicted curves disagree with the other curves but a fair difference was observed between Walker's, Kujawski's and Zhan et al. predictions. It can also be seen in Figure 8 that, Forman's prediction deviates towards the region III resulting in higher Paris constants compared with the other predicted curves. An explanation for this could be due to the effect of accelerated growth rate associated with region III and since only region II is considered in this study, some effect of the unstable region (region III) could contribute to the difference in the derived Paris constants using the Forman's model. Also, the effect of stress level of region III and the associated size of the plastic zone around the crack tip compared with the remaining uncracked ligament of the specimen cannot be ignored. At $R = -1$, Kujawski, Huang and Moan and Zhan et al. models are the only valid correlations out of the five models that were considered in air. It can be seen from Figure 9 that the predicted curve at R of -1 shifted to the right of the baseline indicating that mean stress effect is accounted for. Figure 10 also compares the Kujawski's predicted crack growth rates at $R = 0$, 0.1 and -1 with the experimental data. There is a fair difference between the predicted curves of $R = -1$ and $R = 0$ as shown (Figure 10). However, crack growth rate in this situation should be nearly same as that of $R = 0$.

Also, in fracture mechanics approach to fatigue crack growth; at $R = 0$, $\Delta K = K_{max}$ but at $R = -1$, only the tensile portion of the load cycle is effective and is controlled by K_{max}. Analytically, the common practice is to exclude the compression segment of the loading cycles since there is no crack propagation during the compression portion; and on the assumption that crack closes during compression.

R- ratio effects were considered in seawater by applying the models which are valid for positive and negative stress ratios. The predicted crack growth curves in seawater at R ratios of 0.1 to 0.6 are depicted in Figures 11 and 14, while the predicted curves at R ratio of 0, 0.1 and -1 are compared with the experimental data in Figure 15. At $R = 0.1$, all the modelled curves agree well with the experimental data as shown in Figure 11. Kujawski's and Walker's model also agree at all the positive R ratios. At R ratio of 0.2 (Figure 12), there is a fair difference between Forman's prediction and the other models. Also, at R ratios of 0.4 and 0.6, Forman, Zhan et al. and Huang and Moan's predicted curves deviates from the other two models. These results are shown in Figures 13 and 14. It was observed that Kujawski's and Walker's correlations appear better for positive ratios than the other models.

At $R = 0$ and $R = -1$, it can be seen in that the predicted curves by Kujawski's model are parallel (Red square and green triangular symbols in Figure 15) compared to what was observed in the predicted air curve. Huang and Moan predictions also agree with that of Kujawski at load ratios of 0 and -1. Kujawski's and Zhan et al. models only agree at $R = 0$ but at $R = -1$, there is a fair difference between the two models as shown in Figure 15. However, the predicted curves at $R = 0$ and $R = -1$ for the three applied models shifted to the right of the baseline as expected. Comparing the response derived from the applied models in seawater with respect to that of the baseline, it is worth mentioning that Kujawski's model appears to be more precise for positive and negative stress ratios examined in this study.

The predicted curves in air and seawater are compared in Figures 16 to 19. At R ratio of 0.1 (Figure 16), a response similar to the relationship plotted in Figure 4 was realized as crack growth rates were higher in seawater than in air across all the applied stress intensity factor ranges. The crack growth relationships observed at R ratio of 0.2 is relatively similar to that of Figure 16. However, at R ratios of 0.4 and 0.6 (Figures 18 and 19), it can be seen that the predicted curves in air and seawater are not consistent compared to the predicted curves at R ratios of 0.1 and 0.2 respectively. In Figure 19, it can also be seen that Forman's predicted curve in air nearly converged with the seawater data at higher stress intensity factor range.

Figure 20 shows the predicted low, medium, and high cycle fatigue curves using the material constants derived from the three applied models in seawater at R ratio of -1. This type of prediction should estimate safely the response of the material under reduced operating stress such as that experienced by structures in service. Kujawski's predicted curve was used as the baseline relative to Huang and Moan, and Zhan et al. models as shown (Figure 20). Kujawski's and Huang and Moan predicted curves are parallel to each other for all the three load scenarios. This shows a reasonable agreement between the two models at R ratio of -1. The amount of deviation in the number of loading cycles in the low cycle fatigue (LCF) region was less than a thousand cycle. This could be attributed to the significant levels of plastic deformation which is expected at LCF in most engineering materials.

In medium cycle fatigue (MCF), a difference of ten times greater than what was obtained in the LCF region was observed. The highest deviation in the number of stress cycle was experienced in HCF region with more than half a million cycle difference between the baseline and that predicted by Zhan et al. model. This implies that the effect of applied stress to fatigue crack growth is significantly higher in low cycle fatigue life compared to what occurs in MCF and HCF lives respectively. This appears practical considering the behaviour of offshore structures during service.

From design perspective, a conservative life prediction of these structures is more convincing in fatigue assessment with respect to design life under low load and long life situations (high cycle fatigue). From the procedure described above, the predicted life by Zhan et al. model appears conservative for design, and can represent safely the response of the structures in service since the predicted number of stress cycle is less than that predicted by Kujawski and Huang and Moan models.

6 CONCLUSIONS

Constant amplitude fatigue tests were conducted on Compact Tension specimens in air and in free corrosion conditions. The following conclusions can be drawn from the study

1. Crack growth rates under laboratory simulated seawater are approximately two and four times higher than in air at lower and higher stress intensity factor ranges respectively.
2. The two types of waveform used in air have similar crack growth patterns and presented nearly the same total number of cycles regardless of the loading frequency.
3. The models applied to account for mean stress effects appear better at lower R-ratio than at higher R-ratio. The predicted crack growth rate by Forman's model resulted in higher Paris exponent compared to the other models.
4. Kujawski's model appears to be more precise for positive and negative R-ratios in seawater compared with the other applied models.
5. Low, medium and high cycle fatigue lives were modelled using the predicted material response data obtained at R ratio of −1. Zhan et al. prediction appears conservative for design and can represent the response of the structures to loading conditions similar to what is experienced in service.

ACKNOWLEDGEMENTS

The authors acknowledge the support of the Offshore Wind Structural Lifecycle Industry Collaboration (SLIC) project managed by Centrica Energy (UK) Ltd and of the Petroleum Technology Development Fund (PTDF), Nigeria who support the PhD of Oyewole Adedipe.

REFERENCES

Adedipe, O., Brennan, F. & Kolios, A. Corrosion fatigue load frequency sensitivity analysis. Mar. Struct. In preparation for publication.

Andersen, L. V., Vahdatirad, M. J., Sichani, M. T. & Sørensen, J. D. 2012. Natural frequencies of wind turbines on monopile foundations in clayey soils—A probabilistic approach. Comput. Geotech., vol. 43, pp. 1–11.

ASTM E647-08. 2008. Standard test method for measurement of fatigue crack growth rates.

Bardall, E., Sondenfor, J. & Gartland, P. 1978. Slow corrosion fatigue crack growth in a structural steel in artificial sea water at different potentials, crack depths and loading frequencies. Paper 16 in European Offshore Steels research seminar.

Beden, S. M., Abdullah, S. & Ariffin, A. K. 2009. Review of Fatigue Crack Propagation Models for Metallic Components. European Journal of Scientific Research, vol. 28, no. 3, pp. 364–397.

Berge, S. 1978. Constant amplitude fatigue strength of welds in a sea water drip. Paper 12 in European Offshore Steels research seminar.

Bhattacharya, S., Nikitas, N., Garnsey, J., Alexander, N. A., Cox, J., Lombardi, D., Muir Wood, D. & Nash, D. F. T. 2013. Observed dynamic soil–structure interaction in scale testing of offshore wind turbine foundations. Soil Dyn. Earthq. Eng., vol. 54, pp. 47–60.

Booth, G. S. 1978. Fatigue and corrosion fatigue of welded joints under random loading conditions. Paper 9 in European Offshore Steels research seminar.

Brennan, F.P. 2014. A framework for variable amplitude corrosion fatigue materials tests for offshore wind steel support structures. Fatigue Fract. Eng. Mater. Struct., vol. 37, no. 6, pp. 1–5.

Dinda, S. & Kujawski, D. 2004. Correlation and prediction of fatigue crack growth for different R-ratios using K_{max} and ΔK^{+} parameters. Eng. Fract. Mech., vol. 71, no. 12, pp. 1779–1790.

Elber, W. 1971. The significance of fatigue crack closure. In: Damage tolerance in aircraft structures. ASTM STP 486," Philadelphia.

Forman, R. G. 1972. Study of fatigue crack initiation from flaws using fracture mechanics. Eng. Fract. Mech., vol. 4, no. 2, pp. 333–345.

Haagensen, P. & Dagestad, V. 1978. Random load crack propagation in seawater in a medium- strength structural steel. Paper 22 in European Offshore Steels research seminar.

Haagensen, P., D'Erasmos P., & Petterson, V. 1978. Fatigue performance in air and sea water and fracture of TIG-dressed steel weldments. Paper 8 in European Offshore Steels research seminar.

Huang, X. & Moan, T. 2007. Improved modeling of the effect of R-ratio on crack growth rate. Int. J. Fatigue, vol. 29, no. 4, pp. 591–602.

Kujawski, D. 2001. A new $(\Delta K^{+}\ K_{max})^{0.5}$ driving force parameter for crack growth in aluminium alloys. Int. J. Fatigue, vol. 23, pp. 733–740.

Lombardi, D., Bhattacharya, S. & Muir Wood, D. 2013. Dynamic soil–structure interaction of monopile supported wind turbines in cohesive soil. Soil Dyn. Earthq. Eng., vol. 49, pp. 165–180.

McClung, R. C. 1991. The influence of applied stress, crack length, and stress intensity factor on crack closure. Metall. Trans., vol. 22, no. 7, pp. 1559–1571.

Paris, P. C. & Erdogan, F. 1962. A critical analysis of crack propagation laws. J. Basic Eng., vol. 85, pp. 528–534.

Scott, P.M., Thorpe, T.W. & Silvester, D. R. V. 1983. Rate -determining process for corrosion fatigue crack growth in ferrite steels in seawater. Corros. Sci., vol. 23, no. 6, pp. 559–575.

Solli, O. 1978. Corrosion fatigue of welded joints in structural steels and the effect of cathodic protection. Paper 10 in European Offshore Steels research seminar.

Thorpe, T. W., Scott, P. M., Rance, A. & Silvester, D. 1983. Corrosion fatigue of BS 4360:50D structural steel in seawater. Int. J. Fatigue, vol. 5, no. 3, pp. 123–133.

Walker, K. 1970. The effect of stress ratio during crack propagation and fatigue for 2024-T3 and 7076-T6 aluminium. In: Effect of environment and complex load history on fatigue life. ASTM STP 462. Philadelphia.

Weng, L., Zhang, J., Kalnaus, S., Feng, M. & Jiang, Y. 2013. Corrosion fatigue crack growth of AISI 4340 steel. Int. J. Fatigue, vol. 48, pp. 156–164.

Wildschurt, H., Back, J. de., Dortland, W., & Van Leeuween, J. L. 1978. Fatigue behaviuor of welded joints in air and sea water. Paper 5 in European Offshore Steels research seminar.

Zhan, W., Lu, N. & Zhang, C. 2014. A new approximate model for the R-ratio effect on fatigue crack growth rate. Eng. Fract. Mech., vol. 119, pp. 85–96.